

Interplay between interferences and electron-electron interactions in epitaxial graphene

B. Jouault^{1,2}, B. Jabakhanji¹, N. Camara^{1,3}, W. Desrat¹, C. Consejo¹, J. Camassel^{1,2}

¹*Université Montpellier 2, Groupe d'Étude des Semiconducteurs,
cc074, pl. Eugène Bataillon, 34095 Montpellier cedex 5, France*

²*CNRS, UMR 5650, cc074, pl. Eugène Bataillon,
34095 Montpellier cedex 5, France and*

³*CNM, Campus UAB, Bellaterra (Barcelona), Spain*

Abstract

We separate localization and interaction effects in epitaxial graphene devices grown on the C-face of an 8-^ooff 4H-SiC substrate by analyzing the low temperature conductivities. Weak localization and antilocalization are extracted at low magnetic fields, after elimination of a geometric magnetoresistance and subtraction of the magnetic field dependent Drude conductivity. The electron electron interaction correction is extracted at higher magnetic fields, where localization effects disappear. Both phenomena are weak but sizable and of the same order of magnitude. If compared to graphene on silicon dioxide, electron electron interaction on epitaxial graphene are not significantly reduced by the larger dielectric constant of the SiC substrate.

I. INTRODUCTION

Graphene-based devices are exciting candidates for future generations of microelectronic devices. A promising technique to produce graphene at an industrial scale is the epitaxial graphene growth from a SiC substrate, because these SiC substrates can be patterned using standard lithography methods. Thanks to recent technical improvements, the most delicate and intrinsic features of graphene, those reflecting the chiral nature of the quasi-particles, as, for instance, the so-called 'Half Integer quantum Hall effect'¹⁻⁴ and the weak antilocalization⁵, have been recently reported for epitaxial graphene.

In graphene, depending on the relative magnitude of intervalley scattering time and phase coherence time, either weak localization (WL) or weak antilocalization (WAL) has been predicted⁶. The phase interference correction to the resistance depends on the nature of the disorder. For epitaxial graphene samples, elastic scattering favorable for WAL can be caused by remote charges like ionized impurities in the substrate. On the other hand, atomically sharp disorder (local defects, edges) causes intervalley scattering and gives rise to WL.

Experimentally, in two-dimensional gases, WL is often mixed with electron-electron interaction⁷ (EEI). As WL, EEI gives a correction to the Drude conductivity with a $\ln T$ dependence. It follows that the experimental extraction and separation of EEI and WAL contributions are usually difficult⁸. For graphene, in the diffusive regime, EEI is expected to give this usual temperature dependence correction proportional to $\ln(T)$. EEI is also expected to be sensitive to the different kinds of disorders⁹.

In this work, we take advantage of simultaneous measurements of the longitudinal and transverse resistances to invert the resistivity tensor. We can then separate the different mechanisms which give corrections to the Drude conductivity: i) a geometric contribution, which experimentally appears as a constant term in the longitudinal conductivity; ii) WL and WAL, by a comparison between the experimental magnetoconductance and the Drude magnetoconductivity, iii) EEI, whose temperature dependence can be analyzed in the magnetic field range for which WAL has disappeared.

II. EXPERIMENTAL DETAILS

We have used large and homogeneous single epitaxial graphene layers grown on the C-face of an insulating 8° off-axis 4H-SiC substrate. The graphene sheets have an elongated triangular shape of which quality and homogeneity can be easily checked using micro-Raman spectroscopy. On few selected samples, Cr/Au ohmic contacts were deposited to define Hall-bars with a rough geometry (see inset in Fig.1 for details). Then magneto-transport measurements were done using a 14T magnet in a cryostat and a Variable Temperature Inset operated down to 1.5K. On the best samples, at high magnetic field, the half-integer quantum Hall effect could be observed up to the last plateau in the temperature range 1.5 to 40K. For details, see Ref.¹⁰. In this work we focus on two moderately doped samples (*S1* and *S2*) with dimensions, carrier concentration, mobility and scattering times reported in table I. We work at low injection currents (10nA- $1\mu\text{A}$), mainly at low magnetic fields ($|B| \leq 3\text{T}$), low temperatures (1.5 K-200K) and we focus on the magnetic field dependence of the longitudinal and transverse elements of the resistivity tensor.

III. BACKGROUND CONSIDERATIONS

An overview of the results obtained for sample *S1* is shown in Fig.1. The experimental longitudinal and transverse magnetoresistances $R_{xx}(B)$ and $R_{xy}(B)$ for sample *S1* are presented in Fig. 1a and 1b respectively, at different temperatures between 1.6K and 48K. Let us consider first, Fig. 1a. At low fields ($B \leq 0.1\text{ T}$), a negative magnetoresistance peak centered at $B = 0\text{T}$ is observed in R_{xx} . This peak is typical of weak localization (WL). Indeed, this peak a linear dependence of R_{xx} vs $\ln(T)$ with a slope of the order of h/e^2 (see inset of Fig. 1a) and the amplitude of the peak is $\Delta\rho_{xx} \approx 2\rho_{xx}^2 e^2/h$ (ρ_{xx} is the longitudinal

sample	L	W	n_s	μ	τ_{sr}	τ_{lr}	τ_{tr}	D
<i>S1</i>	5	5	1.1	5000	0.57	0.1	0.065	0.03
<i>S2</i>	40	10	0.8	11000	0.48	0.15	0.11	0.057

TABLE I: for sample *S1* and *S2*: length L between lateral probes, width W (in μm), hole concentration (in 10^{12}cm^{-2}), mobility (in $\text{cm}^2\text{V}^{-1}\text{s}^{-1}$), scattering times τ_{sr} , τ_{lr} and τ_{tr} (in ps) and diffusion constant (in m^2s^{-1}).

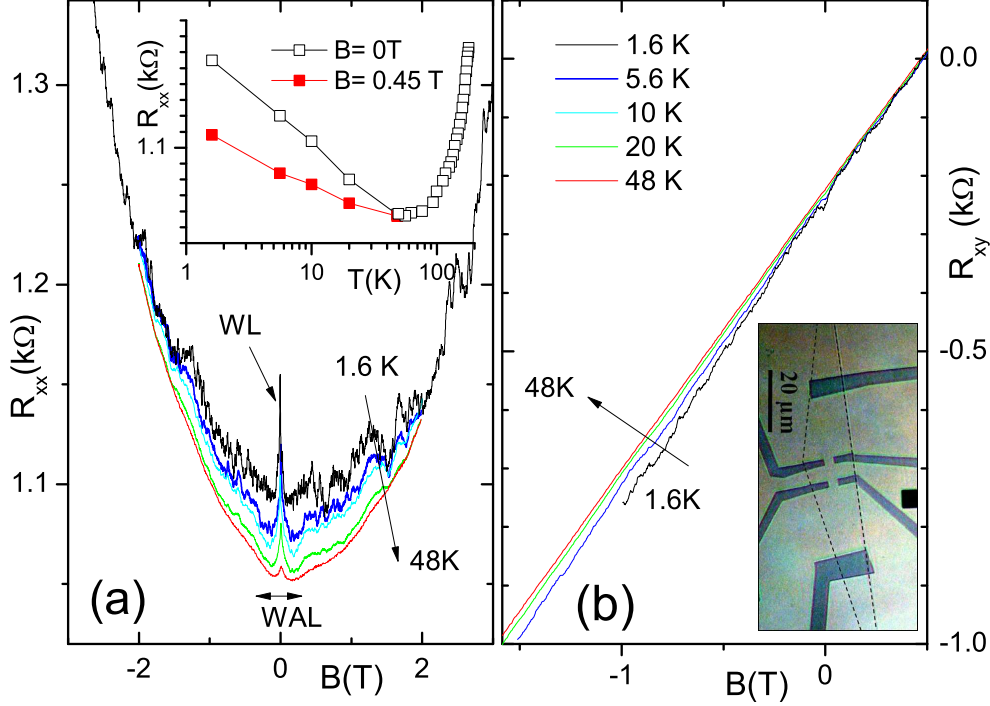


FIG. 1: (color online) (a) $R_{xx}(B)$ at different temperatures for sample $S1$. All curves crosses at $B \approx 2T$ and have a B^2 behavior. Inset shows the temperature dependence of R_{xx} at $B=0$ T (black open squares) and $B=0.45$ T (solid red squares). (b) $R_{xy}(B)$ at different temperatures. The slope of the Hall voltage increases when T decreases due to electron-electron interactions. Inset: photograph of sample $S1$, edges of the graphene layer have been indicated by a dashed line.

resistivity). At higher magnetic fields, reproducible fluctuations in the conductance G are also observed, with amplitudes $\Delta G \approx 0.5e^2/h$ for $S1$ and $\Delta G \approx 0.1e^2/h$ for $S2$.

At magnetic fields $|B| \leq 0.4T$, a smooth depression is observed in R_{xx} , which we attribute to weak antilocalization (WAL). Because this WAL is barely visible in Fig. 1a, we also present additional experimental results in Appendix A. Experimentally, WAL is blurred because fluctuations of conductance are also present, and also because the positive magnetoresistance of the WAL is superposed to another positive magnetoresistance with a pronounced parabolic dependence, which is well observed on the whole magnetic field range $|B| \leq 3T$ presented in Fig. 1a. The theory of weak localization is based on the diffusion approximation and does not hold for magnetic fields much higher than $B_{tr} = \hbar/4eD\tau_{tr} \approx 100$ mT, where τ_{tr} is the transport relaxation time and D the diffusion coefficient. This

means that the parabolic background above B_{tr} should not be attributed to WL features. It must have a different origin. Since the device is being far from having the shape of an ideal Hall-bar (see inset in Fig.1b) we ascribe this parabolic magnetoresistance component to magnetic deflection of the current lines. This is because the lateral probes are invasive and because the graphene layer under the lateral contacts is likely to have different mobility and carrier concentration¹¹. For details, see Annex B.

Beyond geometric and interference corrections, a third correction to the resistivity manifests. It comes from electron-electron interactions and shows as: i) the persistence of a $\ln(T)$ linear temperature dependence of R_{xx} , in a magnetic field range where interference effects are suppressed (see inset of Fig. 1a for a field of $B = 0.45T$); ii) a variation of the Hall slope (Fig. 1b) as a function of T , which cannot be explained by variations of the carrier density, as the hole gas is strongly degenerate ($E_F/k_B T \geq 20$ for $T \leq 50K$, where E_F is the Fermi energy); iii) a crossing of all $R_{xx}(B)$ resistances taken at different temperatures at $B \approx 1/\mu$ (Fig. 1a)¹².

The justification of the last two points, originally given in¹², is as follows. EEI give no correction to the transverse conductance σ_{xy} . It gives a small correction $\delta\sigma^{ee}$ to the longitudinal conductance σ_{xx} . This correction does not depend on B if the magnetic field is smaller than a critical field $B_S \leq \pi k_B T / 2\mu_B$. This condition is fulfilled for all the temperature and magnetic field ranges of this study. Because of this correction, EEI gives rise to a negative magnetoresistance in the first order in $\delta\sigma^{ee} \ll \sigma_{xx}$:

$$\rho_{xx} \sim 1/\sigma_0 - (1 - \mu^2 B^2)\delta\sigma^{ee}/\sigma_0^2 \quad (1)$$

and a variation of the Hall slope $\delta\rho_{xy}/\rho_{xy} \approx -2\delta\sigma^{ee}/\sigma_0$ where σ_0 is the conductivity at $B = 0$. These relations are derived by inverting the conductivity tensor:

$$\rho_{xx} = \frac{\sigma_{xx}}{\sigma_{xx}^2 + \sigma_{xy}^2} \quad (2)$$

$$\rho_{xy} = \frac{\sigma_{xy}}{\sigma_{xx}^2 + \sigma_{xy}^2} \quad (3)$$

It has been established recently⁸ that the separation of EEI and WL⁸ is simplified if the magnetoconductivities $\sigma_{xy}(B)$ and $\sigma_{xx}(B)$ are used, rather than the resistivities. As already stressed, the conductivity of the graphene layer is different below the Cr/Au contacts and, strictly speaking, inverting the resistivity tensor is incorrect because the device is inhomogeneous. However, experimentally, the geometric correction is small, appears only

in the longitudinal magnetoresistance as a parabolic correction, and consequently geometric corrections to the longitudinal conductivity appear as a B -independent shift $\delta\sigma^G$.

The magnetoconductivities for sample $S1$ are plotted in Fig. 2 at different temperatures. The conductivities have been obtained from Eq. 2 and 3, where the resistivities have been estimated by $\rho_{xx} \approx (W/L)(R_{xx}(B) + R_{xx}(-B))/2$ and $\rho_{xy} \approx (R_{xy}(B) - R_{xy}(-B))/2$. The lower inset of Fig.2 shows that all $\sigma_{xy}(B)$ taken at different temperatures collapse on the same curve, as expected for EEI. This also confirms that both mobility and carrier concentration are constant over the whole temperature range and, as the geometric correction only depends on T via the Hall angle μB , that $\delta\sigma^G$ does not depend on the temperature. Finally, the T -independence of the transverse conductivity indicates an effective separation of EEI ($\delta\sigma^{ee}$) and interference ($\delta\sigma^{wl}$) corrections over almost the whole B -range. At low fields $|B| \leq B_{tr}$, a T -dependence of σ_{xy} due to WL is expected but is not observed, being beyond our experimental resolution.

The large decrease of $\sigma_{xx}(B)$ between 0 and 2T in Fig. 2 is due to the magnetic field dependence of the Drude conductivity $\sigma^D = \sigma_0/(1+\mu^2 B^2)$. We express the total conductivity by

$$\sigma_{xx} = \sigma^D + \delta\sigma^{ee} + \delta\sigma^G + \delta\sigma^{wl}. \quad (4)$$

When WL is negligible: $|B| \geq 0.5 \gg B_{tr}$, we impose $\delta\sigma^{wl} = 0$ and Eq. 4, for a given temperature, simplifies as $\sigma_{xx} = \sigma^D + C$, where C is a constant which incorporates both geometric and EEI corrections. This last formula gives very good fits to the conductivity at all temperatures. As an example, the blue dotted line in Fig. 2 is the fit for the $T=5.6K$ data in the interval 0.5-2 T, where σ_0 , μ and C are the fit parameters. Transverse and longitudinal resistivities can be fitted separately but still give very similar mobilities and concentrations, which are reported in Table I.

The upper inset in Fig. 2 is an enlargement of the low- B data at $T = 5.6K$ and evidences the weak antilocalization peak which takes place around the weak localization centered at $B = 0$. A similar weak antilocalization can be detected for all temperatures. The WL theory does not take into account the modification of the current paths due to magnetic field. In other words, before examining the WL contribution to the conductivity, we should first subtract the Drude fits $\sigma^D + C$ (given by the dotted line in Fig. 2) to the observed longitudinal conductivities¹³. Experimental results for samples $S2$ and $S1$ are shown in

Fig. 3, for different temperatures.

IV. CORRECTION DUE TO WEAK LOCALIZATION AND ANTILOCALIZATION

In the diffusive regime in graphene, $\delta\sigma^{wl}$ is given by⁶:

$$\delta\sigma^{wl} = \frac{e^2}{\pi h} \left[F\left(\frac{B}{B_\varphi}\right) - F\left(\frac{B}{B_\varphi + 2B_{sr}}\right) - 2F\left(\frac{B}{B_\varphi + B_{sr} + B_{lr}}\right) \right], \quad (5)$$

where $F(z) = \ln z + \Psi(\frac{1}{2} + \frac{1}{z})$, Ψ is the digamma function, $B_{\varphi, sr, lr} = \hbar/4De\tau_{\varphi, sr, lr}$ and $\tau_{\varphi, sr, lr}$ are the coherence time, the intervalley scattering time and the intravalley scattering time respectively. For simplicity, we identify intervalley to short range (sr) scattering and intravalley to long-range (lr) scattering. We take constant scattering times τ_{sr} and τ_{lr} over the whole temperature range and only τ_φ is allowed to depend on T . Neglecting the warping¹⁴, we also impose $\tau_{lr}^{-1} = \tau_{sr}^{-1} + \tau_{lr}^{-1}$. We then fit the conductivities at different temperatures by Eq. 5. Results are indicated by dashed lines in Fig. 3 (for sake of clarity, fits at high temperatures have not been reported). Best fit is obtained with the values reported in Table I. We estimate the short-range scattering length $L^{sr} = \sqrt{D\tau^{sr}} \approx 100\text{-}140$ nm. The long-range scattering length $L^{lr} = \sqrt{D\tau^{lr}} \approx 70\text{-}90$ nm is even shorter. These lengths are comparable to what is found in exfoliated graphene on SiO₂ substrate¹⁵. They are also comparable to the distance between the SiC steps below the graphene layer. It is often stated that exfoliated graphene is much more disordered at the edge of the SiC steps¹⁶. Therefore step edges could be the main source of scatterings in these samples.

The phase coherence time τ_φ obtained from the fit is plotted in Fig. 4. Apart from a saturation at low T , τ_φ is roughly proportional to $1/T$ between 10K-50K with a slope equal to ≈ 50 ps K for samples $S1$ and $S2$. We conclude that τ_φ obeys the usual temperature dependence for electron electron scattering in the diffusive regime:

$$\tau_\varphi^{-1} = \beta k_B T \ln g / \hbar g, \quad (6)$$

where g is the reduced conductivity: $g = \sigma_0 \hbar / e^2$ and the empirical coefficient β is 1 for $S1$ and 1.4 for $S2$. Similar observations have already been done both for epitaxial⁵ and exfoliated

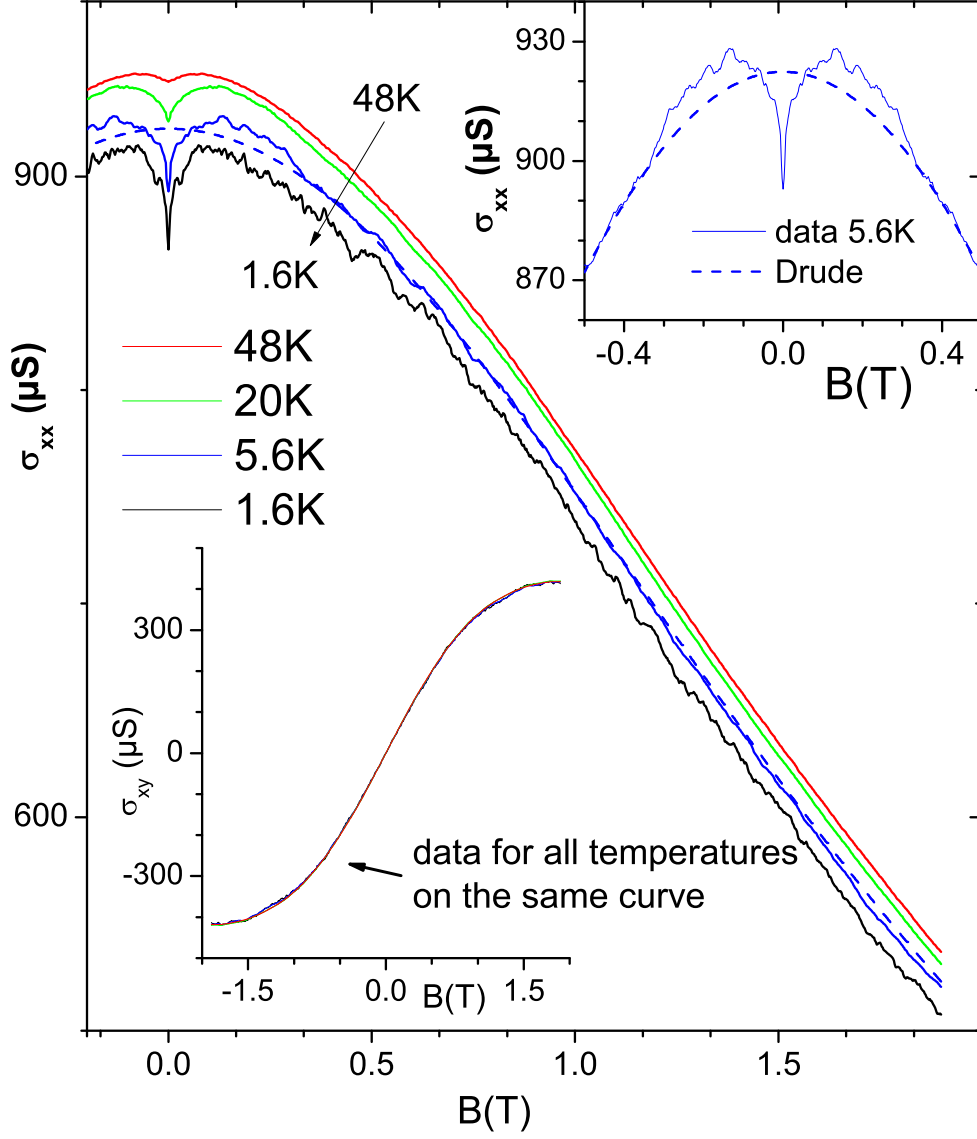


FIG. 2: (color online) longitudinal conductivity σ_{xx} versus B at different temperatures for sample $S1$. Blue dashed line is the best fit of the conductivity at $T=5.6\text{K}$, on a B -interval 0.5-2 T. The fit is done according to $\sigma_{xx}^D(B) + C$ (see text). The upper inset is the enlargement of the area around $B \sim 0\text{T}$. The lower inset shows that all transverse conductivities $\sigma_{xy}(B)$, taken at different temperatures, collapse on a single curve.

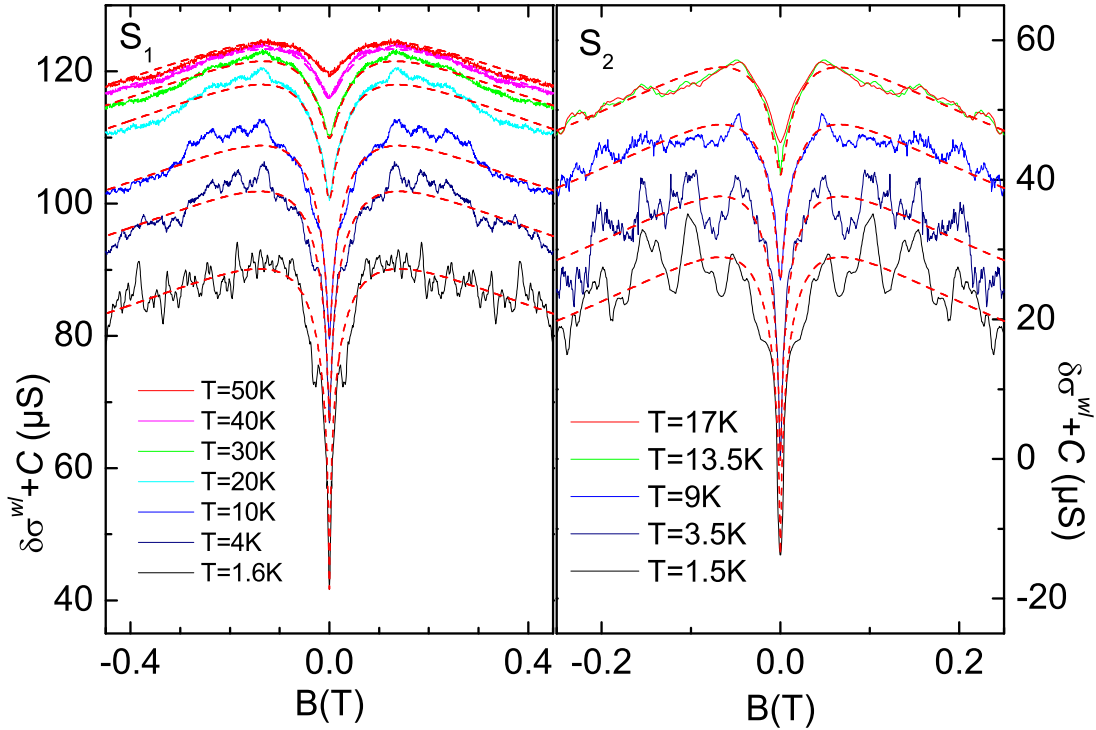


FIG. 3: (color online) (a) Corrections to the conductivities $\delta\sigma^{wl} + C$ at different temperatures for sample S_1 . The T -dependent vertical shift C has been kept for clarity. WL fits according to Eq. 5 are also indicated. (b) Similar analysis for sample S_2 .

graphene^{15,17}. The coherence length $L_\varphi = \sqrt{D\tau_\varphi}$ is readily calculated and plotted in fig. 4b. At low temperature, L_φ slightly exceeds $1\mu\text{m}$.

V. CORRECTION DUE TO ELECTRON ELECTRON INTERACTION

We attribute the temperature dependence of the conductivity to EEI. The Drude mobility is constant over the whole temperature range, therefore there is no temperature dependence of the conductivity induced by electron-phonon scattering. This is not surprising, as the temperature dependence for graphene is small below the Grüneisen temperature T_{BG} given by $T_{BG} \approx 54\sqrt{n_s}$ K, where the concentration n_s is in unit of 10^{12}cm^{-2} ^{18,19}. For our samples, $T_{BG} \approx 54$ K, and almost all our measurements are done below the Grüneisen temperature.

As $k_B T \tau_{tr} / \hbar \ll 1$, we are by definition in the diffusive regime, for which EEI theory

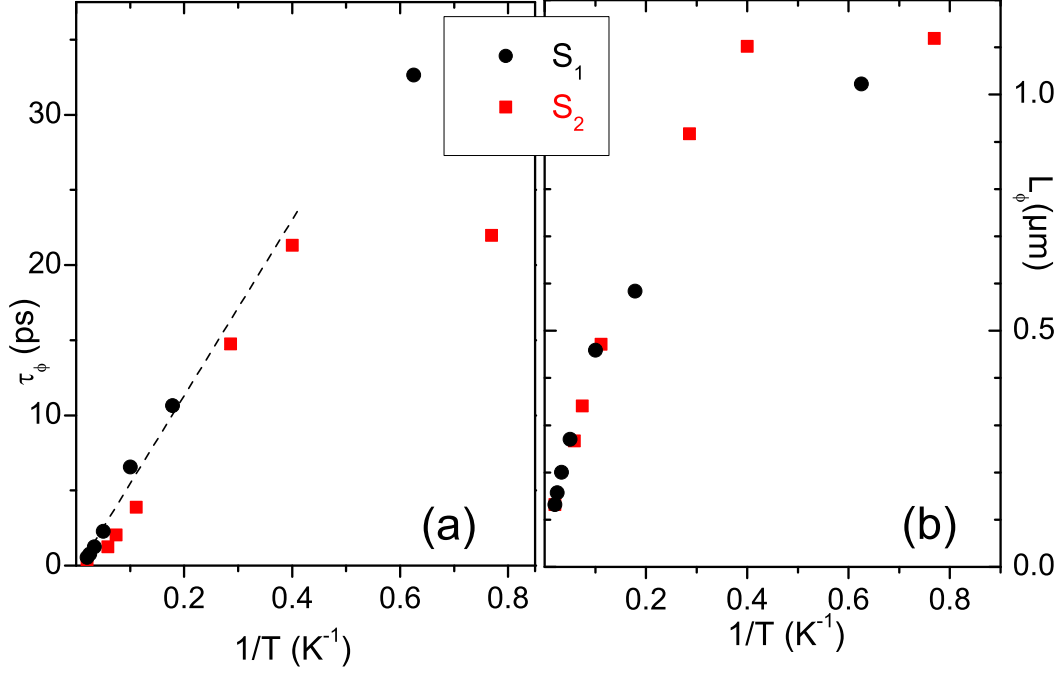


FIG. 4: (color online) (a) phase coherence time τ_ϕ extracted from the fit of the WL, see Fig. 3. Black circles: sample S_1 , red squares: sample S_2 . τ_ϕ is roughly proportional to $1/T$ between 60K and 2.5 K and saturates at lower temperatures. The dashed line is a guide for eyes. (b) Coherence length L_ϕ versus $1/T$, for the two samples.

predicts a temperature dependent correction to the conductivity given by:

$$\Delta\sigma_{ee} = K_{ee} \frac{e^2}{\pi h} \ln \frac{k_B T \tau_{tr}}{\hbar} \quad (7)$$

where K_{ee} is a prefactor whose value depends on the different channels contributing to the EEI⁹. In fig. 5, we show $\delta\sigma_{xx}(T)$ for samples S_2 and S_1 . The expected $\log(T)$ dependence is evidenced and the slope gives $K_{ee} = 0.81 \pm 0.05$ and 0.74 ± 0.07 for samples S_2 and S_1 respectively. These values are very similar to recent experimental findings on exfoliated graphene^{9,20}. In a 2D system with a single valley, K_{ee} takes the form²¹

$$K_{ee} = 1 + c(1 - \ln(1 + F_0^\sigma)/F_0^\sigma) \quad (8)$$

where the unity represents the so-called 'charge' contribution (the Fock and singlet part of Hartree term), the c prefactor is the number of 'triplet' channels (from the Hartree term)

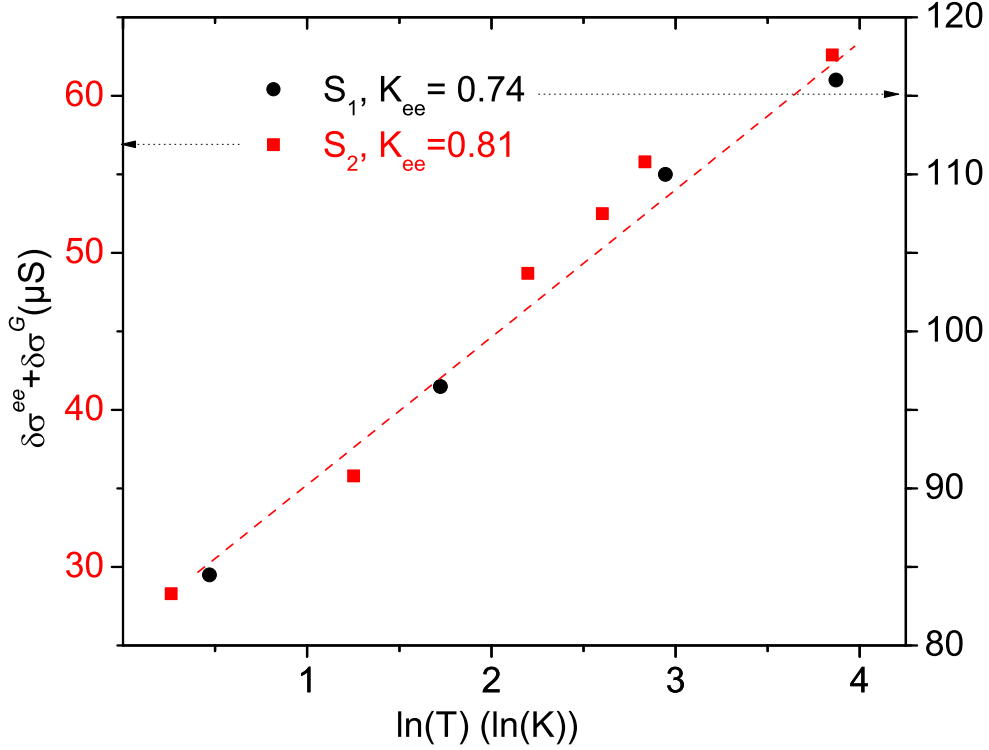


FIG. 5: (color online) experimental temperature dependence of $C(T) = \delta\sigma^G + \delta\sigma^{ee}(T)$ vs $\log(T)$ for samples $S1$ and $S2$. The slope gives $K_{ee} = 0.81$ and 0.74 for $S2$ and $S1$ respectively.

and F_0^σ is the liquid Fermi constant. At low temperatures $k_B T \leq \hbar/\tau_{sr}$ ($T \leq 15$ K for $S2$ and 30 K for $S1$), when long range and short range scattering rates are important, the usual single-valley case is recovered with a prefactor $c = 3$. This leads to $F_0^\sigma = -0.13 \pm 0.04$. This value is small and very close to the value of F_0^σ recently found for exfoliated graphene⁹. This is somehow surprising, as the dielectric constant in SiC (10) is larger than in SiO₂ (3.9) and we would expect even smaller electron-electron interactions because of the screening of the substrate. However, numerical estimation of F_0^σ following, for instance, Ref.⁹ gives $F_0^\sigma \approx -0.09$: a value compatible with our experiment. Also, Ref.²² predicts values for the Fermi liquid constant only slightly smaller than our findings. Interestingly, it was also recently quoted⁹ that at intermediate temperatures $\hbar/\tau_{sr} \leq k_B T \leq \hbar/\tau_{lr}$, additional triplet channels originating from pseudospin conservation (ie valley degeneracy) become relevant and the number of triplet channels increases to $c = 7$. However, we do not observe any change in the slope in Fig. 5 from $T=1.5$ K up to 50 K. The situation is similar in Ref.²⁰, where EEI is observed on a temperature range on which the slope should vary, but where

experimentally the slope remains constant.

To conclude, we show, beyond classical geometric corrections, weak localization, weak antilocalization and electron-electron interactions in epitaxial graphene. Weak antilocalization is observable directly in the resistances, and its analysis gives access to the different scattering times, which are very close to those for exfoliated graphene on SiO₂ substrates. Electron-electron interaction gives also a small correction to the conductivity, which is not significantly smaller than in exfoliated graphene.

We acknowledge the EC for partial support through the RTN ManSiC Project, the French ANR for partial support through the Project Blanc GraphSiC and the Spanish Government for a grant Juan de la Cierva. N. C. also acknowledges A. Bachtold's, A. Barreiro and J. Moser from ICN Barcelona, for technical and theoretical supports.

beginthebibliography22

-
- ¹ T. Shen, J. J. Gu, M. Xu, Y. Q. Wu, M. L. Bolen, M. A. Capano, L. W. Engel, and P. D. Ye, *Applied Physics Letters* **95**, 172105 (2009).
 - ² J. Jobst, D. Waldmann, F. Speck, R. Hirner, D. K. Maude, T. Seyller, and H. B. Weber, *Phys. Rev. B* **81**, 195434 (2010).
 - ³ A. Tzalenchuk, S. Lara-Avila, A. Kalaboukhov, S. Paolillo, M. Syvajarvi, R. Yakimova, O. Kazakova, T. J. B. M. Janssen, V. Fal'ko, and S. Kubatkin, *Nature Nano.* **5**, 186 (2010).
 - ⁴ X. Wu, Y. Hu, M. Ruan, N. K. Madiomanana, J. Hankinson, M. Sprinkle, C. Berger, and W. A. de Heer, *Applied Physics Letters* **95**, 223108 (2009).
 - ⁵ X. Wu, X. Li, Z. Song, C. Berger, and W. A. de Heer, *Phys. Rev. Lett.* **98**, 136801 (2007).
 - ⁶ K. Kechedzhi, E. McCann, H. Suzuura, and B. Altshuler, *Eur. Phys. J. Special Topics* **148**, 39 (2007).
 - ⁷ B. L. Altshuler, A. G. Aronov, and P. A. Lee, *Phys. Rev. Lett.* **44**, 1288 (1980).
 - ⁸ K. E. J. Goh, M. Y. Simmons, and A. R. Hamilton, *Phys. Rev. B* **77**, 235410 (2008).
 - ⁹ A. A. Kozikov, A. K. Savchenko, B. N. Narozhny, and A. V. Shytov, *Phys. Rev. B* **82**, 075424 (2010).
 - ¹⁰ N. Camara, B. Jouault, A. Caboni, B. Jabakhanji, W. Desrat, E. Pausas, C. Consejo, N. Mestres, P. Godignon, and J. Camassel, *Applied Physics Letters* **97**, 093107 (2010).

- ¹¹ B. Huard, N. Stander, J. A. Sulpizio, and D. Goldhaber-Gordon, Phys. Rev. B **78**, 121402 (2008).
- ¹² G. M. Minkov, O. E. Rut, A. V. Germanenko, A. A. Sherstobitov, V. I. Shashkin, O. I. Khrykin, and V. M. Danil'tsev, Phys. Rev. B **64**, 235327 (2001).
- ¹³ Y. Y. Proskuryakov, A. K. Savchenko, S. S. Safonov, M. Pepper, M. Y. Simmons, and D. A. Ritchie, Phys. Rev. Lett. **86**, 4895 (2001).
- ¹⁴ Y.-F. Chen, M.-H. Bae, C. Chialvo, T. Dirks, A. Bezryadin, and N. Mason, Journal of Physics: Condensed Matter **22**, 205301 (2010), URL <http://stacks.iop.org/0953-8984/22/i=20/a=205301>.
- ¹⁵ F. V. Tikhonenko, D. W. Horsell, R. V. Gorbachev, and A. K. Savchenko, Phys. Rev. Lett. **100**, 056802 (2008).
- ¹⁶ B. Jouault, B. Jabakhanji, N. Camara, W. Desrat, A. Tiberj, J.-R. Huntzinger, C. Consejo, A. Caboni, P. Godignon, Y. Kopelevich, et al., Phys. Rev. B **82**, 085438 (2010).
- ¹⁷ S. V. Morozov, K. S. Novoselov, M. I. Katsnelson, F. Schedin, L. A. Ponomarenko, D. Jiang, and A. K. Geim, Phys. Rev. Lett. **97**, 016801 (2006).
- ¹⁸ T. Stauber, N. M. R. Peres, and F. Guinea, Phys. Rev. B **76**, 205423 (2007).
- ¹⁹ E. H. Hwang and S. Das Sarma, Phys. Rev. B **77**, 115449 (2008).
- ²⁰ J. Moser, H. Tao, S. Roche, F. Alzina, C. M. Sotomayor Torres, and A. Bachtold, Phys. Rev. B **81**, 205445 (2010).
- ²¹ N. N. Klimov, D. A. Knyazev, O. E. Omel'yanovskii, V. M. Pudalov, H. Kojima, and M. E. Gershenson, Phys. Rev. B **78**, 195308 (2008).
- ²² M. Polini, R. Asgari, Y. Barlas, T. Pereg-Barnea, and A. MacDonald, Solid State Communications **143**, 58 (2007), ISSN 0038-1098, exploring graphene - Recent research advances, URL <http://www.sciencedirect.com/science/article/B6TVW-4NKXWM7-6/2/79999e036e174b9401e32c27d6501>

VI. APPENDIX A

In Fig. 6, we present magnetoresistances of samples $S1$, $S2$ and of an additional monolayer $S3$, more doped. A straight line αB has been subtracted for sample $S2$, for clarity. For all three samples, a dip is observed on the two sides of the central WL peak. We attribute the dip to WAL.

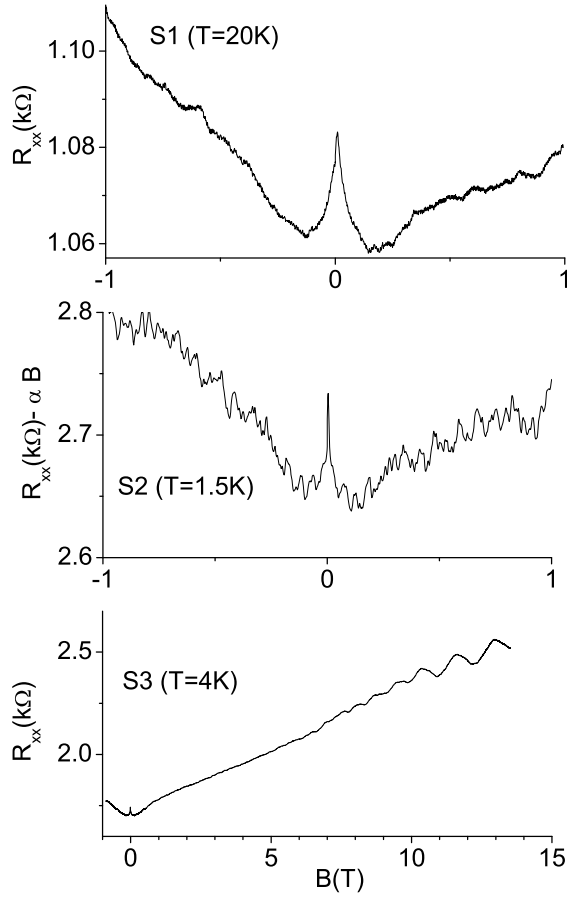


FIG. 6: transverse magnetoresistance for 3 different samples. A small depression attributed to WAL is visible around the WL peak for all three samples.

VII. APPENDIX B

We suggest that most part of the parasitic magnetoresistance comes from the invasive lateral probes. In order to sustain this assumption, classical magnetoresistances can be calculated by means of finite elements method (FEM) for the geometry of the devices. The simplest model only assumes different concentration and mobility under the lateral probes, and the results of this model are shown in Fig. 7 for sample *S1*. There is a good agreement with the experiment for a reduced mobility and an increased concentration under the probes, which seems reasonable if these region have been damaged during the electron beam lithography.

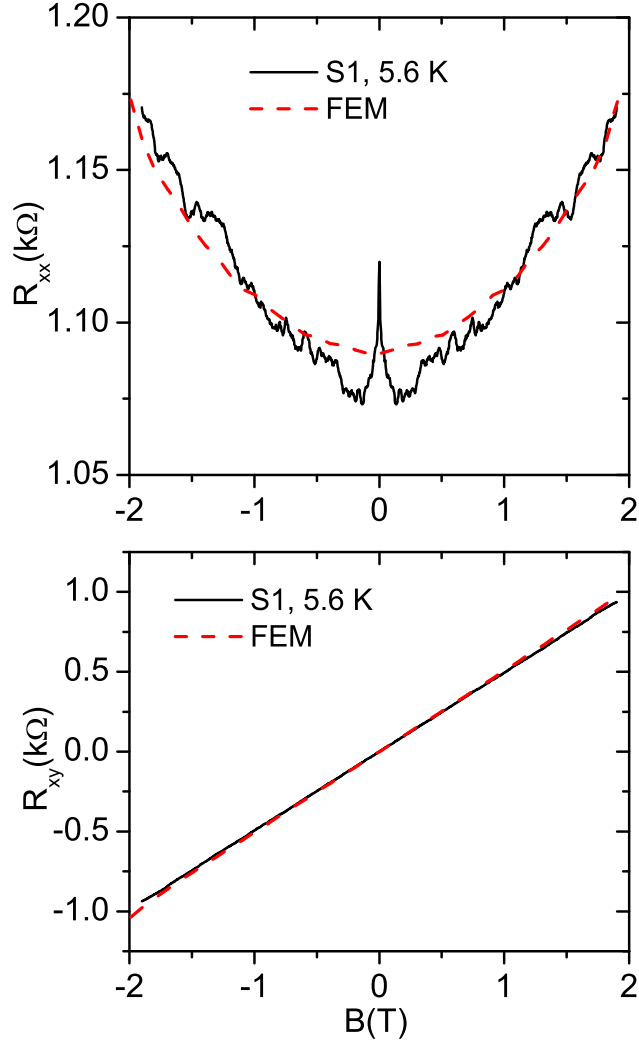


FIG. 7: (color online) experimental longitudinal and transverse magnetoresistances (only symmetric or antisymmetric parts have been kept for clarity) for sample $S1$ are compared to the result of a numerical model based on FEM. The model imposes an increased holes concentration ($n_s = 7 \cdot 10^{12} \text{cm}^{-2}$) and a reduced mobility ($\mu = 0.06 \text{ m}^2 \text{V}^{-1} \text{s}^{-1}$) under the lateral probes. The rest of the graphene layer keeps its parameters as defined in table I.